Faraday Discussions

Accepted Manuscript

This manuscript will be presented and discussed at a forthcoming Faraday Discussion meeting. All delegates can contribute to the discussion which will be included in the final volume.

Register now to attend! Full details of all upcoming meetings: http://rsc.li/fd-upcoming-meetings

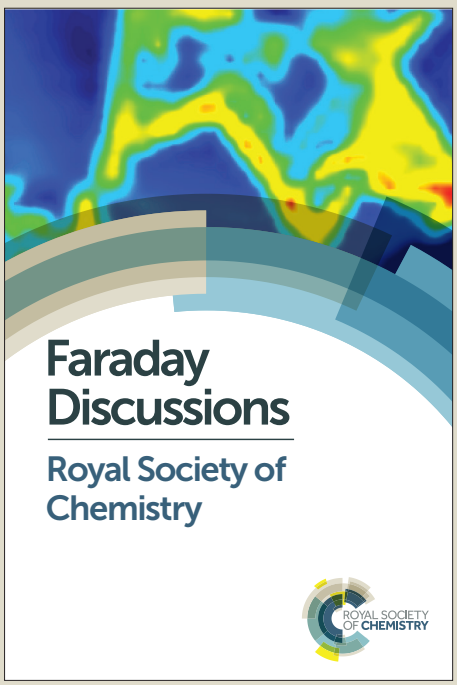

This is an *Accepted Manuscript*, which has been through the Royal Society of Chemistry peer review process and has been accepted for publication.

Accepted Manuscripts are published online shortly after acceptance, before technical editing, formatting and proof reading. Using this free service, authors can make their results available to the community, in citable form, before we publish the edited article. We will replace this *Accepted Manuscript* with the edited and formatted *Advance Article* as soon as it is available.

You can find more information about *Accepted Manuscripts* in the Information for Authors.

Please note that technical editing may introduce minor changes to the text and/or graphics, which may alter content. The journal's standard Terms & Conditions and the Ethical guidelines still apply. In no event shall the Royal Society of Chemistry be held responsible for any errors or omissions in this *Accepted Manuscript* or any consequences arising from the use of any information it contains.

ROYAL SOCIETY OF CHEMISTRY

www.rsc.org/faraday_d

Aggregation and stability of anisotropic charged clay colloids in aqueous medium in the presence of salt

Samim Ali* and Ranjini Bandyopadhyay†

Raman Research Institute, C. V. Raman Avenue, Sadashivanagar, Bangalore 560080, India

Abstract

Na-montmorillonite nanoclay is a colloid of layered mineral silicate. When dispersed in water, this mineral swells on absorption of water and exfoliates into platelets with electric double layers on their surfaces. Even at low particle concentration, the aqueous dispersion can exhibit a spontaneous ergodicity breaking phase transition from a free flowing liquid to nonequilibrium, kinetically arrested and disordered states such as gels and glasses. In an earlier publication [Applied Clay Science, 2015, 114, 8592], we have shown that the stability of clay gels can be enhanced by adding salt later to clay dispersion prepared in deionized water, rather than by adding the clay mineral to a previously mixed salt solution. Here, we directly track the collapsing interface of sedimenting clay gels using an optical method and show that adding salt after dispersing the clay mineral does indeed result in more stable gels even in very dilute dispersions. These weak gels are seen to exhibit transient collapse after a finite delay time, a phenomenon observed previously in depletion gels. The velocity of the collapse oscillates with age of the sample. However, the average velocity of collapse increases with sample age upto a peak value before decreasing at higher ages. With increasing salt concentration, the delay time for transient collapse decreases, while the peak value of the collapsing velocity increases. Using ultrasound attenuation spectroscopy, rheometry and cryogenic scanning electron microscopy, we confirm that morphological changes of the gel network assembly, facilitated by thermal fluctuations, lead to the observed collapse phenomenon. Since clay minerals are used extensively in polymer nanocomposites, as rheological modifiers, stabilizers and gas absorbents, we believe that the results reported in this work are extremely useful for several practical applications and also for understanding geophysical phenomena such as the formation and stability of quicksand and river deltas.

*Electronic address: samim@rri.res.in

†Electronic address: ranjini@rri.res.in

I. INTRODUCTION

Na-montmorillonite is a naturally occurring nanoclay mineral belonging to the smectite group and is available in abundance in nature. The unit particles, known as platelets, of this clay mineral are generally polydisperse in their sizes and shapes, with negative charges on their surfaces and pH dependent positive charges on the edges [1]. The aqueous dispersions of such platelets show spontaneous phase transitions from liquid-like states to nonequilibrium kinetically arrested phases such as glasses and gels [2–6]. The glassy phase has a disordered arrangement of clay platelets stabilized by repulsive interactions, while in the gel phase, the clay platelets assemble into a disordered and volume spanning network structure through attractive bond formation [7]. The formation of such phases, and their rheological and stability behaviors, play a crucial role in many geophysical phenomena such as river delta and quick-sand formation [8, 9]. Besides its fundamental importance in many nonequilibrium phenomena, the understanding of the aggregation and stability of dispersions of colloidal clay particles is also relevant to several technological applications [10–12].

In dry form, the minerals exist in the form of tactoids, which are stacks of clay platelets having thicknesses of the order of nanometers [13]. When these tactoids are dispersed in water, they exfoliate into single platelets in the dilute concentration regime. The degree of exfoliation of the tactoids in an aqueous medium depends on the clay concentration and the ionic conditions of the dispersing medium. In a recent study using a model smectite Laponite, we showed that the exfoliation rate of the tactoids in aqueous dispersion slows down significantly as the dispersion approaches the glass transition. This was attributed to intertactoid repulsions [14]. Our investigation of Na-montmorillonite dispersions shows that the tactoids exfoliate incompletely even below the glass transition concentration due to the reverse osmotic pressure of the hydrated Na^+ counterions in the bulk medium [15]. The presence of added salt in the dispersing medium also inhibits the tactoid exfoliation process. This has an important influence on the stability and the rheological behavior of the resultant dispersions. Above a critical volume fraction of clay particles, the addition of salt in the clay dispersions leads to gel formation. The stability and rheological behavior of the gels with varying salt concentrations depend on the nature of platelet association for attractive bond formation and the strength of these bonds between the platelets. The association of the platelets in the form of overlapping coins (OC) and house of cards (HoC)

configurations contribute significantly to the increasing yield stress of the clay gels upto a critical salt concentration [16]. Above the critical salt concentration, face-face aggregation of clay platelets due to van der Waals attractions is dominant due to considerable charge screening. This increases the thicknesses, and therefore the weights, of the gel strands, thereby making the gels susceptible to gravitational collapse. The concentration of salt in the dispersing medium is therefore a very critical factor in determining the stability of the gels formed from charged colloidal clay particles.

In this paper, we report a detailed study of the stability behavior of Na-montmorillonite clay platelets and their aggregates in dilute aqueous dispersions at different ionic conditions. It is observed that dilute salt-free dispersions, with clay concentration below the glass transition concentration, are not stable under gravity. By directly monitoring the position of the interface of a sedimentating clay gel, we find that a gel that is formed by adding clay powder to a brine solution is also highly unstable under gravity. We demonstrate here that the stability of the dispersions can be enhanced if attractive interactions are induced between the platelets by adding salt *after* dispersing clay in deionized water. The weak gels that are formed remain stable for a duration that depends on the salt concentration in the medium and eventually exhibit transient collapse. Furthermore, the velocity of the collapsing gel is seen to oscillate with increasing gel age, with the average magnitude of the velocity increasing upto a peak value before decreasing subsequently.

The phenomenon of transient collapse was first observed by Poon *el. al.* in 1993 [17] and has been a subject of intense research since then. In the last two decades, the transient collapse phenomenon of colloidal gels has been studied in depletion gels [18–21] and in colloidal gels flocculated at their secondary minima [22, 23]. However, a complete understanding of the microscopic origin of transient collapse remains elusive. Our study, using a combination of rheological measurements, ultrasound attenuation spectroscopy and cryogenic scanning electronic microscopy, reveals that the continuous restructuring and association of the platelets in overlapping coin configurations lead to increase in the widths and lengths of the gel network strands. We argue that a competition between the gravitational stresses on these network strands and the local yield stresses plays an important role in determining the stability of gels formed from charged colloidal clay particles.

II. EXPERIMENTAL SECTION

A. Material Structure:

Na-montmorillonite is a natural smectite clay mineral having 2:1 layered phyllosilicate structure [1]. A unit layer, known as a platelet, consists of an aluminum octahedral sheet sandwiched between two tetrahedral silica sheets. The flat surfaces (the basal planes) of the platelet acquire negative charges due to the isomorphic substitution of Al^{+3} ions in the octahedral sheet by Mg^{+2} and Fe^{+2} ions. The negative charges thus arising on the basal surfaces are compensated by exchangeable intercalated Na^{+} counterions. The edges of the platelet have pH dependent positive charges [24]. The thickness of a single-layer platelet is around 1 nm, while its lateral sizes can vary from tens of nanometers to a few micrometers. In dry form, when the negative charges on the basal surfaces are neutralized by the exchangeable Na^{+} counterions, several platelets assemble in a stack, known as a tactoid, under the influence of van der Waals attraction. In an aqueous medium, the Na^{+} counterions get hydrated due to the absorption of water molecules in the intratactoid spaces. As a result, tactoids slowly swell and exfoliate, producing laminar flexible platelets with electric double layers (EDLs) on their surfaces [25]. The highly polydisperse nature of the sizes and shapes of the Na-montmorillonite platelets can be seen in the representative SEM micrograph in the inset of Fig. 1. The lateral sizes of these platelets, calculated from the SEM micrographs, vary from tens of nanometers to a few micrometers with an average lateral size of 420 nm (Fig. 1).

B. Sample preparation

Na-montmorillonite powder used in this work was purchased from Nanocor, Inc. The powder is baked for 24 hrs in an oven at 120°C to remove absorbed moisture. The powder is next dispersed in water using a magnetic stirrer under vigorous stirring conditions. Three batches of samples are prepared at different ionic conditions as noted below:

Samples without salt: Clay powder is dispersed in highly deionized Milli-Q water of resistivity 18.2 MΩ.cm. The dispersion is stirred for seven days before using it for experiments.

SBC sample: Clay powder is dispersed in brine solution. The brine solution is prepared by adding a predefined amount of NaCl in Milli-Q water. The mixture is kept under stirring

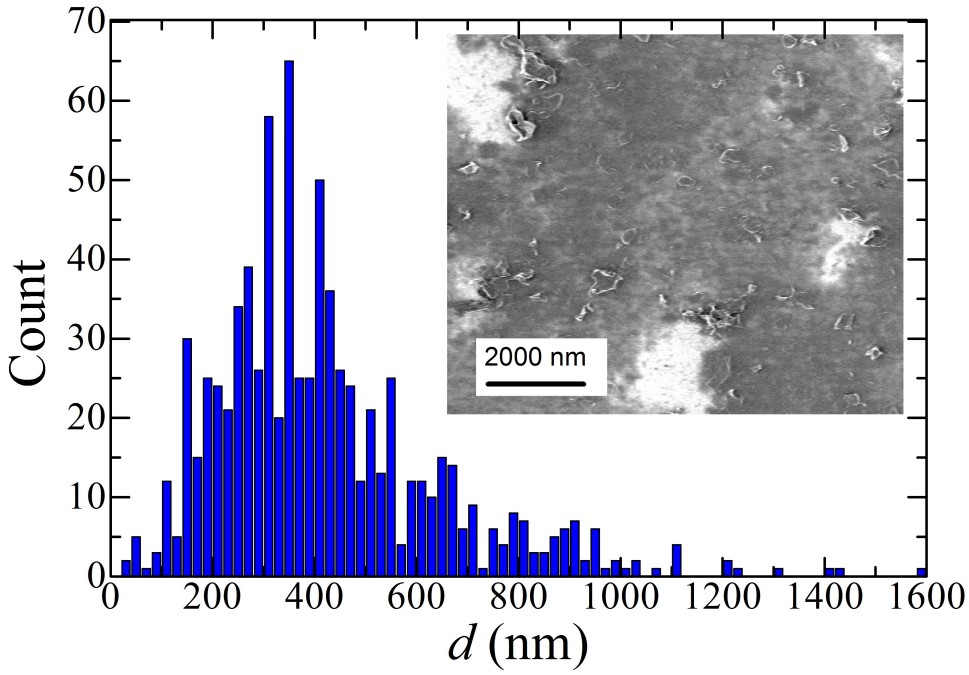

FIG. 1: Lateral size distribution of Na-montmorillonite platelets measured using SEM. Calculation of the platelet size distribution is done with more than 700 single layers identified in SEM micrographs. The average lateral size calculated from the distribution is 420 nm. Inset shows a representative SEM micrograph containing Na-montmorillonite platelets.

conditions for seven days before experiments. We designate such a sample as SBC (Salt added Before Clay).

SAC sample: A predefined amount of salt is added after seven days to a clay dispersion prepared in a salt free condition. The mixture is further stirred for three hours before experiments. We designate such a sample as SAC (Salt added After Clay).

C. Experimental arrangements:

1. *Light based experimental setup*

A homemade light based experimental setup, shown in Fig. 2 (a), is used to monitor the sedimentation of clay dispersions. A schematic diagram of this setup is shown in Fig. 2 (b). A linear light source made from red LEDs (midband wavelength=633 nm) is housed

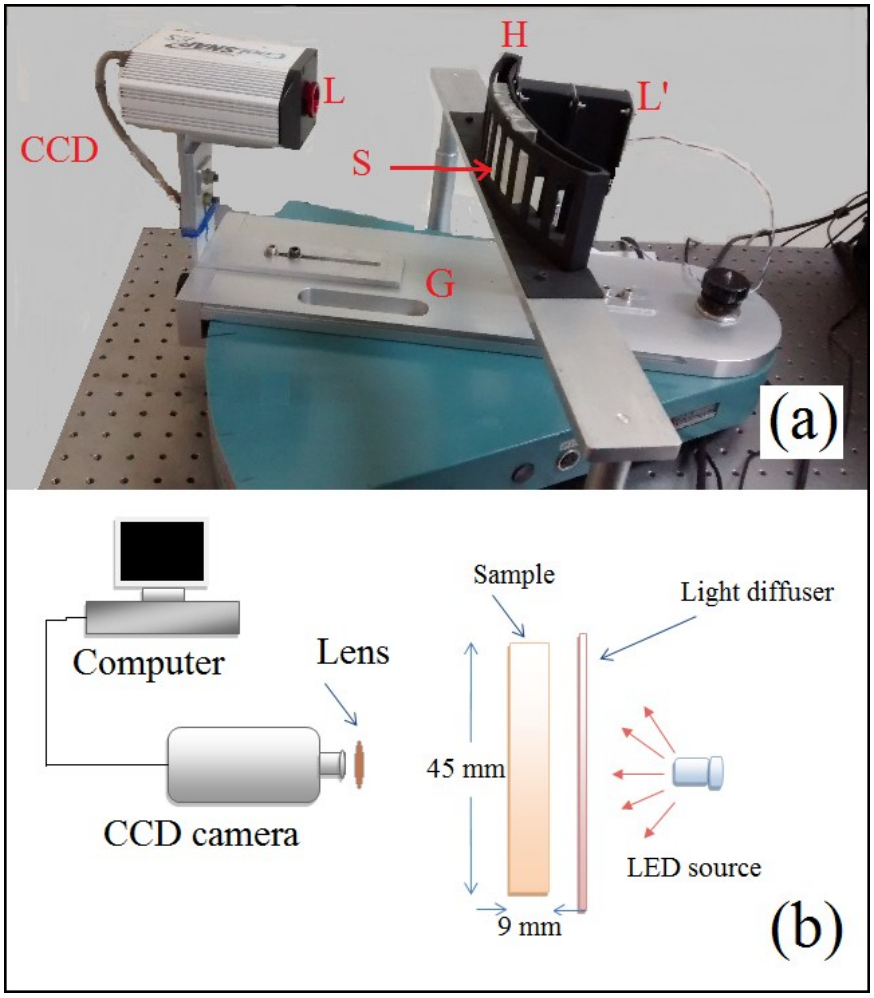

FIG. 2: (a) Snapshot of the light based experimental setup used for the sedimentation study. The main components of this setup are − a light source (L′), sample cuvettes (S), cuvette holder (H), goniometer (G), CCD camera and lens assembly (L). (b) Schematic diagram of the experimental setup.

within a rectangular box (L′) containing two layers of light shaping diffusers procured from Luminit^{TM}. This arrangement produces a homogeneous and diffused light source which is used to illuminate the samples. The intensity of the diffused light is controlled by changing the current to the LEDs. Rectangular glass cuvettes (S) of inner dimensions 10 mm (w) X 9 mm (d) X 48 mm (h) are used to hold the clay dispersions. The cuvettes are then housed in a cuvette-holder (H) fixed to the goniometer (G) arm. Cuvettes containing the samples of height $h_0 = 45$ mm are sealed using a silicone sealant to prevent evaporation of water. The temperature of the sample is kept constant at 25±0.2°C. The diffused light

is incident perpendicularly to the cuvette wall. The light transmitted through the sample is collected using a CCD camera (Photometrics CoolSnap ES, Roper Scientific Inc.) and a lens (L). A regular sequence of images is captured at different ages t_s of the sample. t_s=0 is defined as the time at which the stirring of the sample is stopped inside the sample cuvette. The intensity of the incident light is adjusted so that the transmitted intensity detected by the CCD camera remains below the saturation level of the CCD sensor. The CCD images are finally analyzed using Winview and Matlab softwares. The transmitted intensity I_{tr} at each pixel of the CCD image is measured in terms of the grey value. To eliminate the spatial inhomogeneity of the incident light, the value of I_{tr} at each pixel of the CCD image is normalized by the background intensity of light that passes through clear water.

2. Rheological measurements

Rheological measurements are performed at 25±0.1°C using a stress controlled rheometer (Anton Paar MCR501) with a concentric cylindrical measuring head of length 25 mm and diameter 16.6 mm. The sample is kept in a cylindrical container of inner diameter 27.6 mm and length 42 mm. The measuring head is inserted into the sample upto 25 mm from the top surface of the sample. After loading the sample, an oscillatory strain of amplitude 1000% and angular frequency 10 rad/s is applied for two minutes to shear melt the sample. A small oscillatory strain of amplitude 0.1% and angular frequency 6 rad/s is subsequently applied to the sample to monitor the evolution of the elastic modulus G' and the viscous modulus G'' with sample age t_s. Here, $t_s = 0$ is defined as the time at which the shear melting of the sample is stopped in the measuring cell.

3. Scanning Electron Microscopy (SEM)

A field effect scanning electron microscope (ULTRA-PLUS FESEM) from Carl Zeiss is used to scan clay platelets dried on an ITO (indium tin oxide) coated glass plate. The ITO surface, made hydrophilic by keeping the glass plate in a solution of H_2O_2, NH_3OH and water in the ratio 1:3:7 at a temperature of 80°C for 5 hrs, is washed with deionized water and dried. A 10 μL drop of 0.5% w/v Na-montmorillonite dispersion is spread on the hydrophilized ITO-glass plate and dried very fast (within 10 seconds) in an oven at a

temperature of 200°C to avoid coagulation of the clay tactoids. Data acquisition and size measurements are carried out using SmartSEM (Carl Zeiss) and ImageJ softwares.

4. Cryogenic scanning electron microscopy

For cryo-SEM characterization, Na-montmorillonite dispersions with different salt concentrations, C_s, are loaded in glass capillary tubes (procured from Hampton Research, USA) of bore size 1 mm. The ends of the capillaries are then sealed. Samples are then kept in an undisturbed condition for different ages t_s. The samples are then vitrified using liquid nitrogen slush of temperature −200°C. The vitrified samples are fractured and sublimated for 30 mins at a temperature −90°C and then coated with a thin layer of platinum (thickness approximately 1 nm) at a temperature −150°C in vacuum using a cryotransfer system (PP3000T from Quorum Technologies). The imaging of these samples is then performed using the ULTRA-PLUS FESEM from Carl Zeiss at an electron beam strength of 2 KeV.

5. Size measurement using ultrasound attenuation spectroscopy

Clay particle size distributions at different ionic conditions are estimated by measuring the ultrasound attenuation spectra (attenuation coefficient α_v *vs* ultrasound frequency ω) and ultrasound speeds using a DT-1200 acoustic spectrometer (procured from Dispersion Technology Inc). The details of this technique can be found in the literature [14, 26]. For each attenuation measurement, 130 ml of the clay dispersion is loaded in a cell containing two identical ultrasound transducers facing each other. The attenuation spectra are measured at different ionic conditions of the colloidal dispersions by varying the ultrasound frequency in the range 3 to 99.5 MHz and for 12 different sample widths ranging from 5 mm to 20 mm. A sample temperature of 25±0.2°C is maintained for each measurement. The unimodal particle size distribution (PSD) of the dispersed clay is estimated from the attenuation spectrum using an analysis algorithm developed by the manufacturer. The theory of viscous attenuation of ultrasound, which was used to fit the attenuation data, is described in Section I of the ESI‡. The parameter values that were used to calculate PSDs are supplied in Section II of the ESI‡.

6. Electroacoustic measurements

Electroacoustic measurements are used to indirectly track the positions of the collapsing interfaces at higher clay concentrations. The technique is explained in detail in Section III of the ESI‡. The results obtained from the electroacoustic measurements are used for comparison with the optical tracking data of the collapsing interfaces reported here for dilute clay concentrations. A photograph of the electroacoustic setup is provided in Fig. S1 of the ESI‡.

III. RESULTS AND DISCUSSION

We first monitor the stability of clay platelets in dilute aqueous salt-free dispersions using the light transmission method. Fig. 3 shows the variation of the transmitted intensity (I_{tr}) along the height, h, of the cuvette for a 0.8% w/v aqueous dispersion of Na-montmorillonite clay at several t_s values. Here, t_s is the time since stirring of the sample is stopped and $h = 0$ is at the bottom of the sample cuvette. At age $t_s = 0$, I_{tr} remains almost constant with varying h. This indicates that the clay platelets are distributed uniformly in the dispersion. For $t_s > 0$, I_{tr} increases with h. A representative CCD image of the sample acquired at $t_s = 59$ hrs is shown in the inset (a) of Fig. 3. The I_{tr} vs h data can be fit to $I_{tr}(h) = I_0 + I'\exp(h/h'_0)$, where I_0, I' and h'_0 are the fitting parameters. h'_0 is a length scale characterizing the intensity gradient, and therefore is a measure of the particle concentration gradient, along the sample height. At low h, a sharp decrease in I_{tr} can be observed due to the deposition of the clay platelets at the bottom of the sample cuvette. The positions where the I_{tr} data deviate from the exponential fits correspond approximately to the clay sediment heights and are indicated by arrow heads in Fig. 3. At larger h, the exponential variation of I_{tr} with h indicates a continuously varying concentration of platelets along the height of the sample. As a result of the wide size distribution of the clay platelets (Fig. 1), the bigger platelets settle faster than the smaller ones. The smaller particles diffuse out over larger length scales with increasing t_s, giving rise to a gradual increase in h'_0 with age as observed in the inset (b) of Fig. 3. The absence of any distinct interface between the supernatant and the clay rich region [inset (a) of Fig. 3] confirms the absence of a gel phase [27, 28].

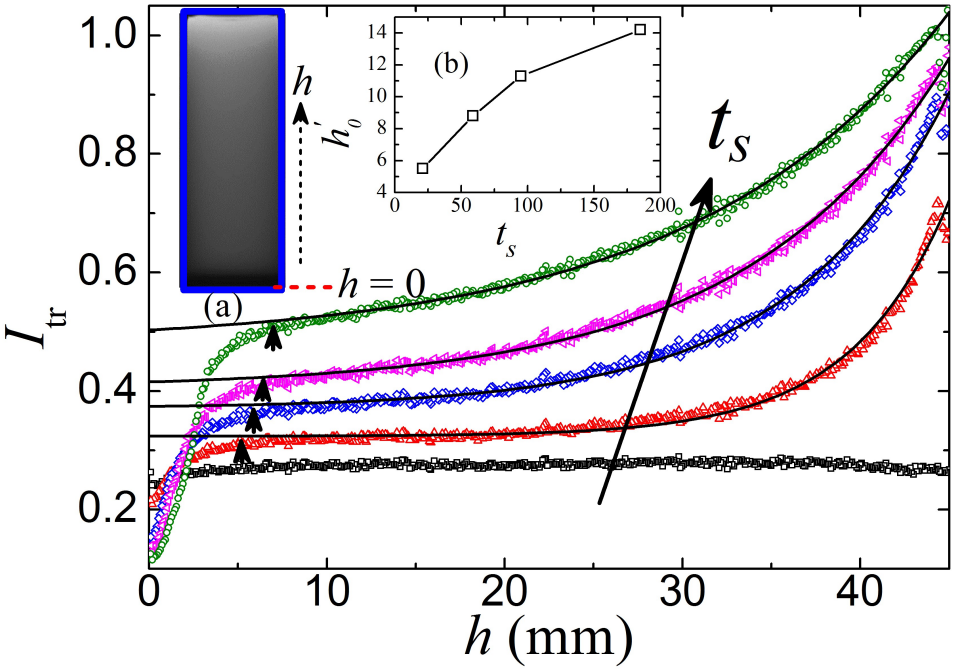

FIG. 3: Variation of the transmitted intensity (I_{tr}) along the height h of the cuvette for a 0.8% w/v Na-montmorillonite dispersion at ages t_s = 0, 21, 59, 95 and 185 hrs (bottom to top). Here, $h = 0$ is at the bottom of the sample column and $t_s = 0$ is defined as the time when the stirring of the sample in the cuvette is stopped. The arrow heads indicate the positions of the top surfaces of the sediment at different t_s. The solid lines are the exponential fits $[I_{tr}(h) = I_0 + I'\exp(h/h_0')]$ to the data. Here, h_0' is a length scale characterizing the particle concentration gradient. The inset (a) shows an image of the sample acquired at t_s = 59 hrs using the CCD camera. The variation of h_0' with t_s is shown in the inset (b).

Due to the high concentration of negative charges on the basal surfaces and the wide lateral sizes of Na-montmorillonite platelets, there is a small spillover of negative potential onto the positive edges of the platelets in dispersions of pH>7 [29–31]. As a result, the effective potential on the edges are also negative. Hence, the Na-montmorillonite platelets in dilute dispersions, such as the ones reported in Fig. 3, do not show any aggregation and sediment under gravity. However, salt-free aqueous dispersions of Na-montmorillonite clay platelets exhibit strong stability above the glass transition concentration (4% w/v) of the sample. In this higher concentration regime, the clay dispersions are stabilized by

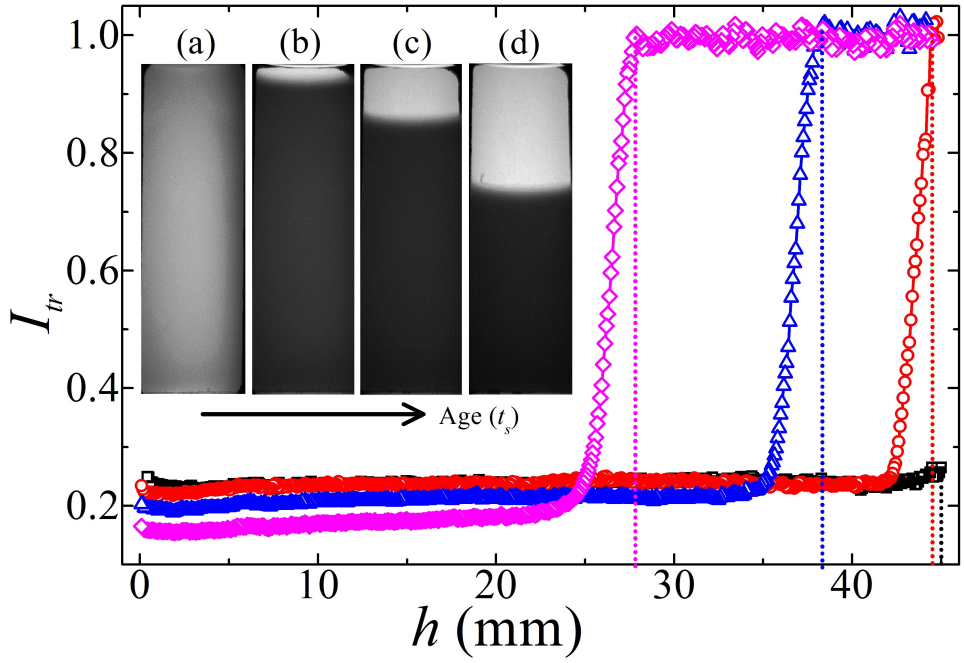

FIG. 4: Variation of the transmitted intensity (I_{tr}) with sample column height, h, of a 0.8% w/v Na-montmorillonite dispersion (SAC) with 60 mM salt at ages t_s = 0.5 hrs (□), 3 hrs (○), 10 hrs (△) and 95 hrs (◊). The corresponding CCD images of the gel at different t_s are shown in the insets (a), (b), (c) and (d). The vertical dotted lines indicate the positions of the interface between the supernatant and the collapsing gel at different t_s.

long range repulsive interactions and form kinetically constraint, structurally disordered soft glasses [14, 15]. This has been probed using the electroacoustic method (Fig. S1 of the ESI‡) and the results are plotted in Fig. S2 of the ESI‡.

We next investigate the assembly and stability behaviors of dilute clay dispersions in the presence of added salt. Attractive interactions between the clay platelets in a 0.8% w/v Na-montmorillonite dispersion are induced by the addition of salt to the medium which results in the reduction of the Debye screening lengths characterizing the Na-montmorillonite platelets in the dispersions. CCD images captured at different ages (t_s) of a 0.8% w/v Na-montmorillonite dispersion (SAC) with 60 mM salt, prepared by adding salt to the dispersions after dispersing clay powder in deionized water, are shown in the insets of Fig. 4. At t_s = 0.5 hrs, the transmitted intensity, I_{tr}, remains constant with varying h (□ in

Fig. 4), indicating that the clay particles are uniformly distributed along the sample height. At higher t_s, a distinct interface between the clear supernatant and the clay rich phase appears in the dispersion, with the transmitted intensity through the supernatant reaching 100% at decreasing values of h with increasing sample age. The positions of the interface at different ages are shown by dotted lines in Fig. 4.

Representative time evolution data of the normalized positions h/h_0 of the interfaces in 0.8% clay dispersions with 40 mM salt, prepared at two different ionic conditions (SBC and SAC), are shown in Fig. 5. Here, h_0 is the total sample height. It is seen in this figure that the sample designated as SBC (□), prepared by dispersing clay powder at a concentration

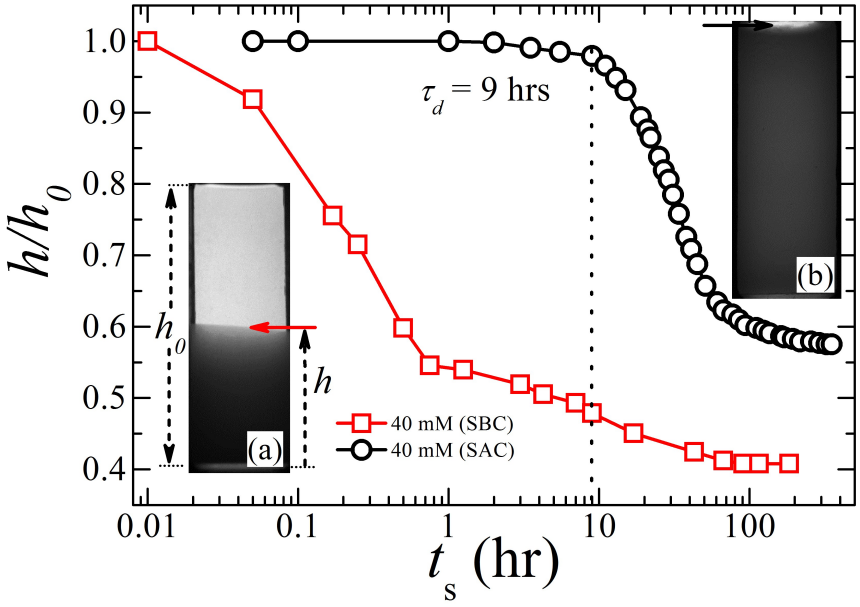

FIG. 5: Variation of the normalized height, h/h_0, of the interface between the clear supernatant and the collapsing gel versus age, t_s, in a 0.8% w/v Na-montmorillonite dispersion (SBC), prepared by adding clay powder in 40 mM brine (□), and a 0.8% w/v Na-montmorillonite dispersion (SAC), prepared by adding 40 mM salt after dispersing the clay powder (○). Here, $h = 0$ is at the bottom of the sample column and $t_s = 0$ is defined as the time when stirring of the sample is stopped in the cuvette. The delay time, $\tau_d = 9$ hrs, for the onset of collapse of the SAC sample is indicated by the vertical dotted line. The insets (a) and (b) show the CCD images acquired at $t_s = 10$ hrs of the SBC and SAC gels respectively.

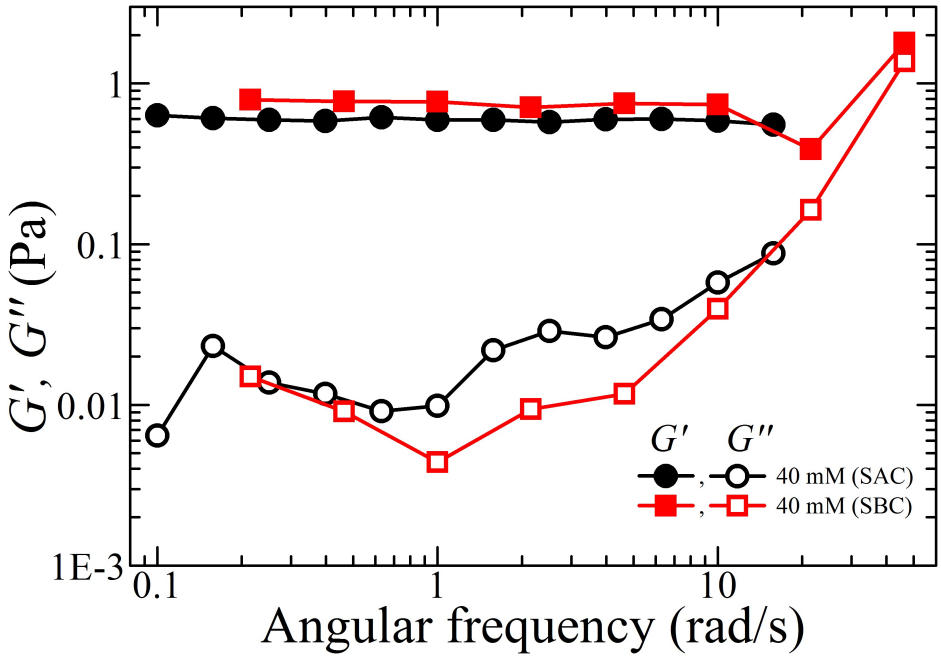

FIG. 6: Frequency dependence of storage modulus G' (solid symbols) and loss modulus G'' (empty symbols) of the SBC sample (□), prepared by dispersing 0.8% w/v Na-montmorillonite clay powder in 40 mM salt solution, and the SAC sample (○), prepared by adding 40 mM salt to a 0.8% w/v Na-montmorillonite dispersion. An oscillatory shear strain of amplitude 0.1% was applied in these experiments.

of 0.8% w/v in a 40 mM salt solution, is highly unstable under gravity, with the normalized interface height (h/h_0) decreasing continuously with t_s. On the other hand, the sample designated as SAC (○ in Fig. 5), prepared by adding 40 mM salt in the 0.8% w/v clay dispersion, remains stable under gravity for a finite delay time, $\tau_d = 9$ hrs, during which the interface remains in a quiescent state. At $t_s > \tau_d$, the interface height of the SAC sample decreases rapidly with t_s due to a transient collapse phenomenon and eventually saturates at longer times.

To understand the microstructures of these dispersions, we perform frequency sweep rheological experiments for samples at $t_s = 30$ min by varying the imposed oscillatory frequency in the range 0.1−50 rad/s at a strain amplitude of 0.1%. The frequency sweep measurement could not be extended to very low frequencies for the SBC gel due to the

unstable nature of this sample. The SAC gel, in comparison, is stable for a very long duration, allowing data collection even for very small oscillatory frequencies. It is seen from Fig. 6 that the that elastic modulus G' is much higher than the viscous modulus G'' for both the samples. Furthermore, G' is almost independent of the applied oscillatory frequency, whereas G'' is weakly dependent on frequency for values less than 10 rad/s. These are typical rheological signatures exhibited by kinetically arrested colloidal particles in dispersion [32]. Since the clay concentration (0.8% w/v) investigated here is well below the glass transition concentration (4% w/v) [15], the observed kinetic arrest clearly arises from the formation of gel network structures that are facilitated by attractions between the clay platelets induced by the added salt. Indeed, the formation of clay gels has been verified by us using direct visualization methods and will be discussed in detail later.

To understand the observed stability behavior of these gels prepared at identical clay and salt concentrations, we estimate the particle size distributions (PSDs) of the clay particles in their dispersions using ultrasound attenuation spectroscopy. The size measurements are performed while stirring the dispersions using a magnetic stirrer to avoid sedimentation of the particles. Fig. 7 shows the measured attenuation spectra in the ultrasound frequency range $3 - 99.5$ MHz for 0.8% w/v Na-montmorillonite dispersions with 40 mM salt concentration prepared for the two different ionic conditions (SBC and SAC) described earlier. The attenuation spectra are fitted to the theoretical estimates for the attenuation spectra (solid lines in Fig. 7) considering a unimodal size distribution [Eqns. S1−S6 (Section I) of the ESI‡]. The particle size distributions thus estimated from these spectra are plotted in the inset of Fig. 7. It is seen that the equivalent spherical median sizes are $d_{SBC} = 54$ nm for the SBC sample (□ in Fig. 7) and $d_{SAC} = 41$ nm for the SAC sample (○ in Fig. 7). The average thickness of tactoids in the SBC sample is therefore higher than that in the SAC sample. The lower degree of exfoliation of tactoids in the SBC sample arises due to the presence of salt in the dispersing medium during the preparation stage. The salt present in the water reduces the osmotic pressure difference of the hydrated Na^+ counterions between the intratactoid spaces and the bulk medium. This inhibits the diffusion of the native Na^+ counterions from the intertactoid spaces into the bulk water, thereby reducing the rate of exfoliation of the clay tactoids and leading to larger particle sizes in the SBC sample [15]. Owing to large d_{SBC} values, the gravitational stress on the SBC gel network dominates over the local yield stress and eventually leads to the rapid gravitational collapse of the gel im-

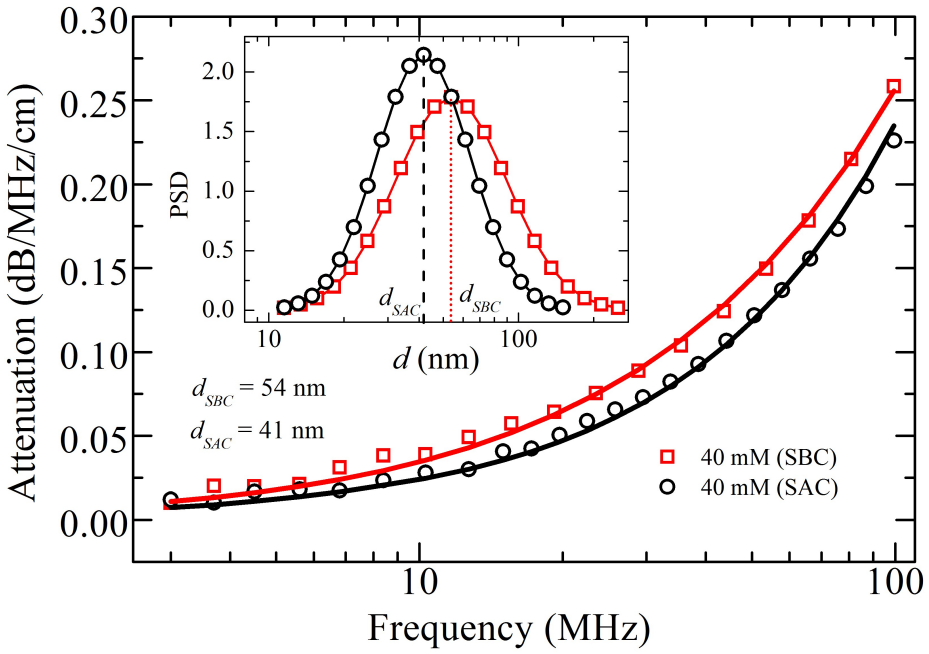

FIG. 7: Ultrasound attenuation spectra measured in the frequency range of $3 - 99.5$ MHz at $t_s = 0$ for a 0.8% w/v Na-montmorillonite dispersion (SBC sample), prepared by adding the clay powder in 40 mM brine (□), and for a 0.8% w/v Na-montmorillonite dispersion (SAC sample), prepared by adding 40 mM salt after dispersing the clay powder in water (○). Solid lines are theoretical fits to the attenuation spectrum using Eqns. S1−S6 (Section I) of the ESI‡ for a unimodal size distribution of the clay particles. The inset shows the corresponding particles size distribution of the two samples. It is seen that $d_{SBC} = 54$ nm and $d_{SAC} = 41$ nm are the median values for the equivalent spherical sizes of the particles in the dispersions prepared in SBC (□) and SAC conditions (○) respectively.

mediately after stirring is stopped. In contrast, the degree of exfoliation in the SAC sample (○ in Fig. 7) is higher, resulting in a larger number of exfoliated particles in this dispersion compared to the SBC sample. Hence, the network connectivity in the SAC sample is expected to be higher. At the same time, the gravitational stress on the gel network in the SAC sample is comparatively weaker due to the smaller sizes of the constituent particles. In contrast to the SBC gel, a quiescent or steady state of the SAC sample can therefore be observed upto a delay time $\tau_d = 9$ hrs (○ Fig. 5).

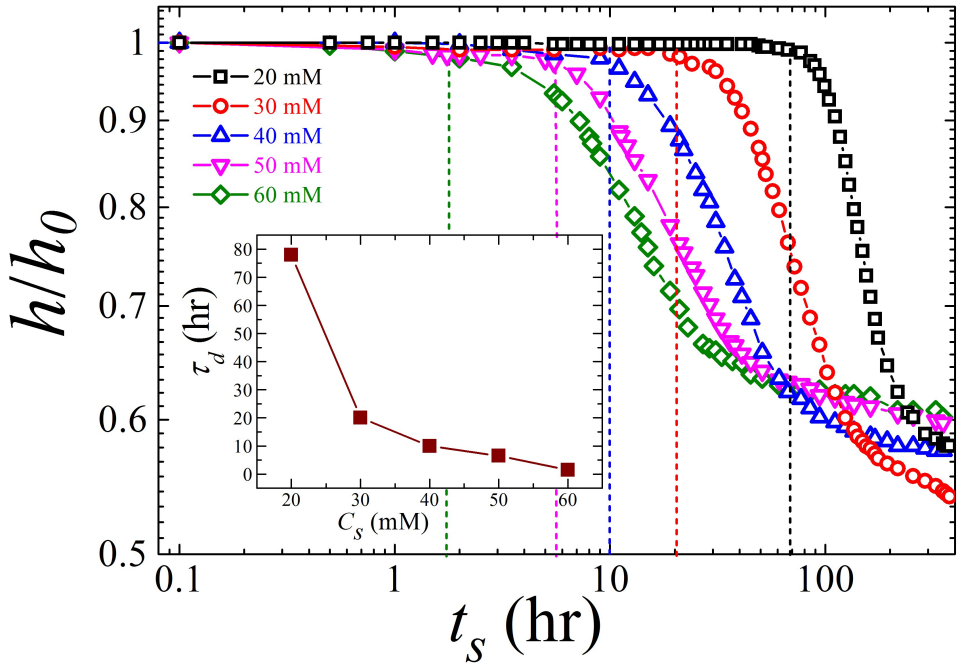

FIG. 8: Evolution of the normalized heights, h/h_0, of the interface between the clear supernatant and the collapsing gel versus age, t_s, of 0.8% w/v Na-montmorillonite dispersions (SAC) with salt concentrations of 20 mM (□), 30 mM (○), 40 mM (△), 50 mM (▽) and 60 mM (◊). Gelation is induced in these samples by dispersing clay powder in deionized water and then adding salt. The inset shows the variation of the delay time, τ_d, with varying salt concentrations. The vertical dashed lines indicate the positions of the delay time, τ_d, for the different salt concentrations.

The sedimentation data for 0.8% Na-montmorillonite dispersions prepared under SAC conditions with varying salt concentrations C_s are shown in Fig. 8. All samples here exhibit quiescent regimes followed by collapse regimes. When C_s is increased, the delay time τ_d decreases (inset of Fig. 8), indicating faster collapse of the gels. To better describe the collapse process, we calculate the velocity, v_{int}, of the collapsing interface (Fig. 9) from the I_{tr} versus t_s data (Fig. 8) for different C_s. Irregular oscillations in the values of v_{int} with t_s can be seen during collapse. It is seen that the average magnitude of v_{int} increases with t_s and shows a peak before decreasing at higher t_s. It is also observed that the peak shifts to lower t_s for higher salt concentrations. This observation will be discussed later.

The variation of the elastic modulus G' with t_s is next measured by applying a small

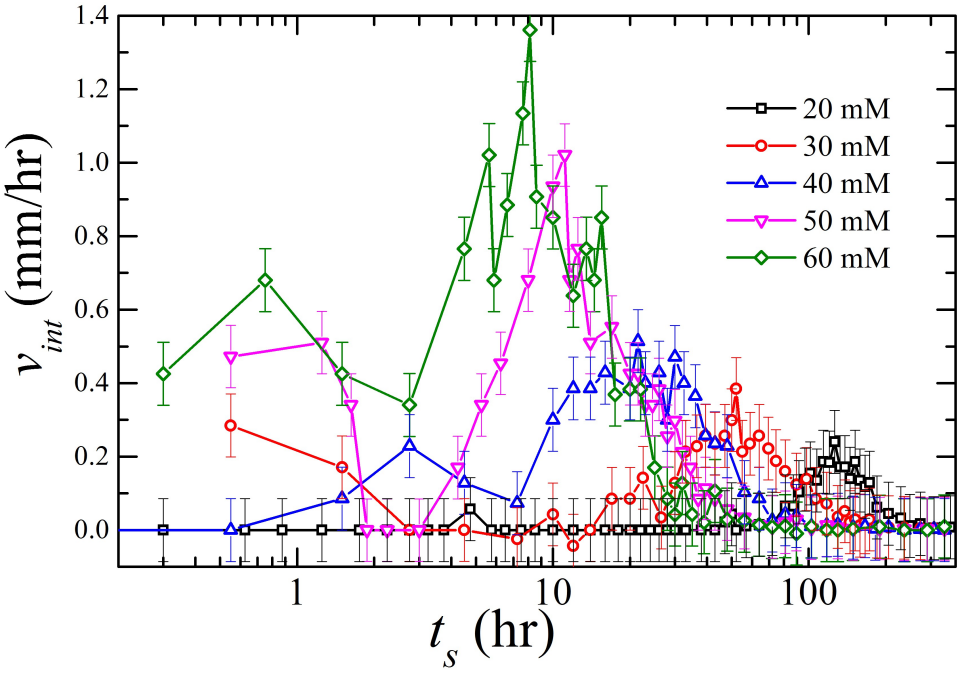

FIG. 9: Plot of the collapse velocity, v_{int}, of the interface with age t_s for 0.8% w/v Na-montmorillonite dispersions (SAC) at salt concentrations 20 mM (□), 30 mM (○), 40 mM (△), 50 mM (▽) and 60 mM (◊). The error bars quantify the systematic errors that arise from the detection of the interface using the optical method described earlier.

oscillatory strain of amplitude 0.1% and angular frequency 10 rad/s to samples prepared under SAC conditions with salt concentrations 20 mM, 40 mM and 60 mM. These data are shown in Fig. 10. It is seen that G' increases monotonically upto age $t_s = t_r$ (indicated by arrows in Fig. 10 for different salt concentrations). This is followed by a slight decrease in G', with the data showing oscillations as t_s is increased further. However, the average magnitude of G' increases with t_s. The variations of t_r (time at which the first oscillation in G' is observed) and the delay time, τ_d, measured from the interface collapse profile (Fig. 8) are plotted in the inset of Fig. 10. These two characteristic times show very good agreement with each other for all C_s values. This suggests that during the quiescent period ($t_s < \tau_d$), G', and hence the yield stress of the gel, both increase. However, a mechanical failure of the gel network occurs at $t_s = t_r \sim \tau_d$, leading to transient collapse.

When C_s is increased, the platelets constituting the gels are expected to aggregate faster

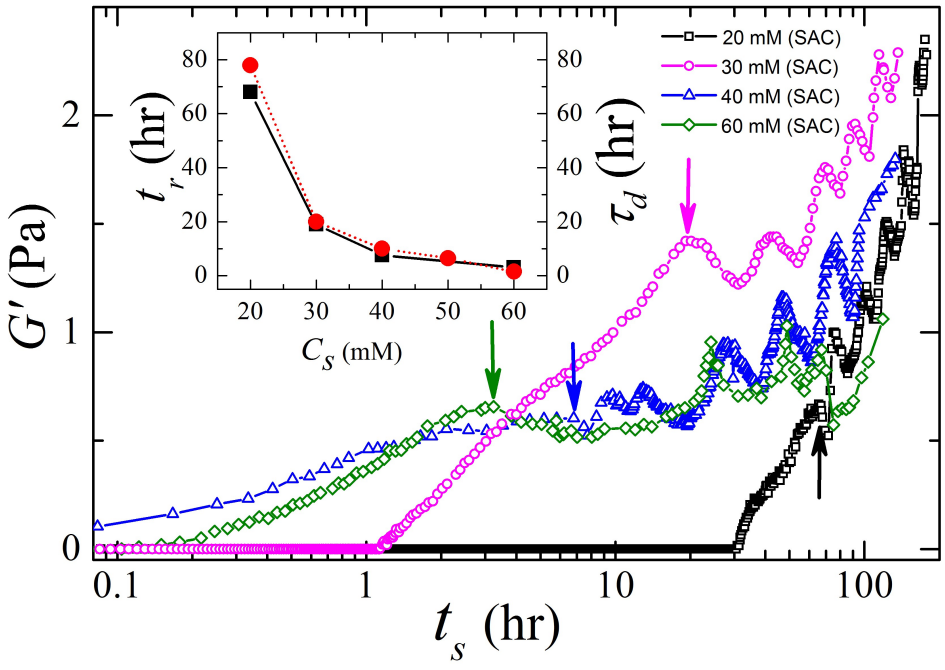

FIG. 10: Evolution of the elastic modulus, G', with age, t_s, of 0.8% w/v Na-montmorillonite (SAC) dispersions at salt concentrations 20 mM (□), 30mM (○), 40 mM (△) and 60 mM (◊). The moduli are measured by applying an oscillatory strain of amplitude of 0.1% and angular frequency of 10 rad/s. The arrows indicate the positions of the delay times, t_r, at which G's start exhibiting oscillations for all four salt concentrations. The inset shows the plot of t_r (■) and τ_d (●) with varying salt concentration.

through the formation of stronger attractive bonds [16]. The weights of the gel strands increase substantially as a result, accelerating the transient collapse of the gels (inset of Fig. 10). Once transient collapse is initiated, the gel strands approach each other. This gives rise to even faster platelet aggregation. This, in turn, leads to an increase in the gravitational stress on the gel network, with the velocity of the collapsing interface increasing sharply with t_s as observed in Fig. 9. However, due to gel compaction and the formation of progressively stronger bonds between the particles in the network, the yield stress also increases simultaneously during the sedimentation process and eventually overcomes the gravitational stress. This results in a decreasing interface velocity at large t_s values. The competition between the gravitational and yield stress on the gel gives rise to a repetitive

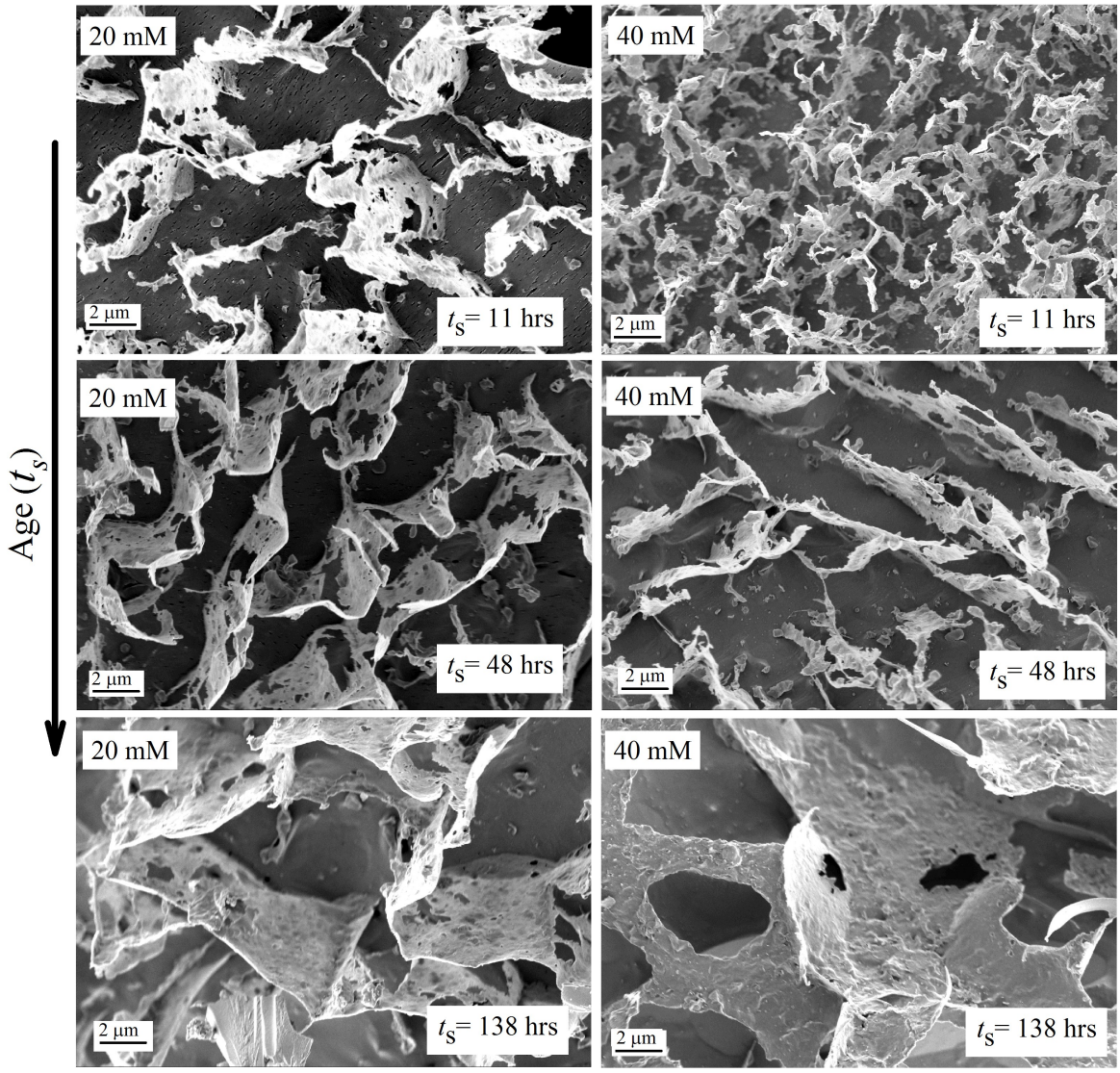

FIG. 11: Representative micrographs obtained using cryo-SEM for 0.8% w/v Na-montmorillonite dispersions (SAC) with $C_s = 20$ mM (left panel) and 40 mM (right panel) at ages $t_s = 11$ hrs, 48 hrs and 138 hrs (top to bottom). The scale bars represent 2 μm.

process of mechanical failure and build up of the gel structure in the collapse regime and results in the observed oscillations of v_{int} and G' at $t_s > t_r \sim \tau_d$.

To understand the mechanical failure of the gel network with age, we directly study the variation of the microscopic structures of the aging gels using cryogenic scanning electron microscopy (cryo-SEM). Fig. 11 shows the cryo-SEM micrographs of the weak SAC gels formed with $C_s = 20$mM and 40 mM at $t_s = 11$ hrs, 48 hrs and 138 hrs. It is seen from

these images that the clay platelets form highly disordered network structures. It is clearly observed that the average lengths and widths of the network strands are higher than the average lateral size of each clay platelet (420 nm reported in Fig. 1). This indicates that the platelets in the network structures are connected in overlapping coin (OC) configurations [33]. In an OC configuration, the positive edge of a platelet is attached to the negative basal surface near the edge of another platelet in a parallel fashion (Fig. 4 in [16]). It is also clearly visible from the images in Fig. 11 that the widths and lengths of the network strands grow with age as an increasing number of platelets participate in network formation through OC configurations. This suggests that the gels restructure continuously due to thermal fluctuations and reorient in a way that eventually leads to the formation of stronger attractive bonds [34]. As a result, the elastic modulus, and hence the yield stress, increase continuously with age upto a time $t_r \sim \tau_d$ as observed in the rheological measurements earlier (Fig. 10). On the other hand, due to the increase in the dimensions of the network strands as observed in Fig. 11, the gravitational stresses on the network strands increase simultaneously with t_s. At $t_s = \tau_d$, the gravitational stresses overcome the local yield stresses of the gels leading to mechanical failure and the subsequent collapse of the gels as presented in Fig. 8 and Fig. 10. In the SBC gel samples, on the other hand, the network strands are thicker and longer, and the gravitational stress typically always exceed the local yield stress, resulting in accelerated gel collapse (Fig. 5).

IV. CONCLUSIONS

In this work, we have studied the aggregation and stability behaviors of charged anisotropic clay particles of Na-montmorillonite in aqueous dispersions at a concentration (0.8% w/v) well below that required to achieve the glass transition. Microscopic imaging using scanning electron microscopy shows that the clay platelets are highly polydisperse in their shapes and sizes (Fig. 1). We show that these platelets are not stable in salt-free aqueous dispersions in the dilute concentration regime and sediment under gravity with a particle concentration gradient along the sample height that gets more pronounced with sample age (Fig. 3).

We next investigate the stability of gels formed by inducing attractive interactions between the clay platelets in a dilute concentration regime by directly monitoring the gel

interface in optical transmission experiments. Attraction is induced by screening the negative charges on the basal surfaces of the platelets by adding salt in the medium. The gels prepared by dispersing clay powder in NaCl solutions are not stable under gravity and collapse immediately with a distinct interface between the clear supernatant and a clay-rich sediment (the SBC gel indicated by □ in Fig. 5). In contrast, we report remarkable enhancement of the stability of the dispersions if identical amounts of salt are added to the clay dispersions after adding the clay powder to water (the SAC gel indicated by ○ in Fig. 5). We further observe that the SAC gel is stable for a finite delay time and eventually exhibits transient collapse under gravity with a sharp interface height that decreases with increasing ages (Fig. 5).

In the collapse regime, the velocity of the collapsing interface exhibits oscillations with sample age (Fig. 9). The average velocity of the interface increases with age upto a peak value before decreasing at higher ages. With a systematic increase in the salt concentration, the delay time for transient collapse decreases (Fig. 8), while the average collapse velocity increases (Fig. 9). The microscopic mechanism involved in the observed transient collapse is investigated using rheological measurements and with direct visualization of the gel microstructures using cryogenic scanning electron microscopy. It is seen that the elastic modulus G' of the gel increases with sample age upto a time t_r (Fig. 10), indicating the growing attractive strength of the gel network. The G' data shows oscillations at ages higher than t_r for all salt concentrations investigated here. The times, t_r, at which the oscillations in G' start are found to be in good agreement with the delay times τ_d for transient collapse (inset of Fig. 10).

The direct visualization of the microscopic structures at different salt concentrations and ages of the gels confirms that the gels undergo microscopic restructuring with time (Fig. 11), thereby attaining higher elastic moduli and hence yield stresses with age since preparation. During the restructuring process, an increasing number of platelets is seen to participate in network formation through overlapping coin (OC) configurations (Fig. 12(a)). This leads to increase in the lengths and widths of the network strands (Fig. 12(b)). The gravitational stress on the gel strands increases as a result and eventually overcomes the local yield stress after a delay period. This leads to the mechanical failure of the network strands and the subsequent transient collapse of the gels (Fig. 12(c)). During the collapse, the gravitational stresses on the gel network increase further due to the coarsening of the gel strands as they

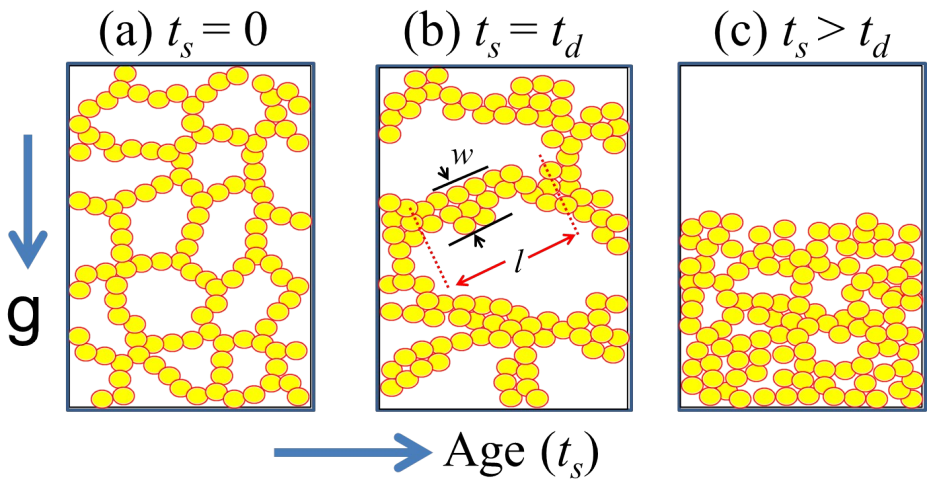

FIG. 12: Schematic of a clay gel under gravity (the direction is shown by an arrow pointing downward) illustrating the evolution of network morphology and collapse with age, t_s. (a) A gel network dominated by overlapping coin (OC) configurations of clay platelets at a time immediately after preparation, (b) increase in the widths (w) and lengths (l) of network strands at higher ages due to the rearrangement of platelets, and (c) the collapsed state of the gel network at age $t_s > t_d$.

approach each other. This results in a further increase in the velocity of collapse. The processes of gradual gel compaction during sedimentation and the continuous restructuring lead to a substantial increase in the local yield stresses of the gel network. A condition eventually arises in which the yield stresses characterizing the network strands overcome the gravitational stresses, resulting in a decrease in collapse velocity at higher ages (Fig. 9). Such competition between the local yield stresses and the gravitational stresses on the gel network strands during gel collapse leads to oscillations in the interface collapse velocity (Fig. 9), and in the elastic modulus (Fig. 10).

Further insight into the transient gel collapse phenomenon reported here can be obtained by theoretically modelling the experimental data acquired in this work. To model the observed delayed gel collapse and the subsequent densification, two important microscopic quantities, the association rate K_A and the dissociation rate K_D of the clay platelets, have to be measured and combined in a poroelastic model of the collapsing gel. However, the dependences of the quantities K_A and K_D on the sample age, its exfoliation state, the salt

concentration and the local volume fractions are extremely non-trivial and need to be first quantified accurately.

It is important to conclude by noting that our study of the stability behavior of clay dispersions at a higher clay concentration (3% w/v) in the presence of added salt using electroacoustic methods (Section III and Fig. S1 of the ESI‡) shows similar stability behaviors of SBC and SAC gels (Fig. S3 of the ESI‡) as observed in the dilute concentration regime studied here. However, it is seen for the 3% w/v gel that its yield stress dominates over the gravitational stress for relatively longer time durations due to the higher network connectivity and the slower rearrangement processes at higher clay concentrations.

Finally, we would like to point out here that the Na-montmorillonite used for this study belongs to the naturally occurring phyllosilicate group of clay minerals and is an important component of soil. We therefore believe that the results presented here on the tactoid exfoliation, aggregation and stability behaviors of aqueous dispersions of these minerals at different ionic conditions will be very useful in understanding many geophysical phenomena such as the formation of river deltas and the collapse of quicksand [8, 9]. On the other hand, our observations of the collapse behavior in salt-stabilized colloidal clay particle dispersions also demonstrate the ubiquity of the transient collapse phenomenon previously only observed in depletion gels [18–21] and in colloidal gels flocculated at their secondary minima [22, 23].

V. ACKNOWLEDGMENT

We thank Mr. A. Dhasan and Mr. K. M. Yatheendran for their help with cryo-SEM imaging and Prof. V. A. Raghunathan for loaning us the goniometer used in this work. We also thank Mr. T. R. Venketesh for his help during sample preparation and data collection.

FOOT NOTE:

‡Electronic supplementary information (ESI) available: theory used for PSD measurement using ultrasound attenuation spectroscopy (Section I), supplied parameter values to estimate PSDs (Section II), the electroacoustic setup used in this work (Section III and Fig. S1), plot of I_{CVI} versus t_s for varying clay concentrations (Fig. S2) and plot of I_{TVI} versus

t_s for varying salt concentrations (Fig. S3).

[1] F. Bergaya and G. Lagaly, in *Handbook of Clay Science*, ed. F. Bergaya and G. Lagaly, Elsevier, 2013, vol. 5, pp. 1 – 19.

[2] S. Abend and G. Lagaly, *Applied Clay Science*, 2000, **16**, 201 – 227.

[3] R. Bandyopadhyay, D. Liang, H. Yardimci, D. A. Sessoms, M. A. Borthwick, S. G. J. Mochrie, J. L. Harden and R. L. Leheny, *Physical Review Letters*, 2004, **93**, 228302.

[4] B. Ruzicka and E. Zaccarelli, *Soft Matter*, 2011, **7**, 1268–1286.

[5] D. Saha, Y. M. Joshi and R. Bandyopadhyay, *Soft Matter*, 2014, **10**, 3292–3300.

[6] E. Paineau, L. J. Michot, I. Bihannic and C. Baravian, *Langmuir*, 2011, **27**, 7806–7819.

[7] E. Zaccarelli and W. C. K. Poon, *Proceedings of the National Academy of Sciences*, 2009, **106**, 15203–15208.

[8] A. Thill, S. Moustier, J.-M. Garnier, C. Estournel, J.-J. Naudin and J.-Y. Bottero, *Continental Shelf Research*, 2001, **21**, 2127 – 2140.

[9] A. Khaldoun, E. Eiser, G. Wegdam and D. Bonn, *Nature*, 2005, **437**, 635–635.

[10] F. Uddin, *Metallurgical and Materials Transactions A*, 2008, **39**, 2804–2814.

[11] H. H. Murray, *Applied Clay Science*, 2000, **17**, 207 – 221.

[12] Y. Liu, M. Zhu, X. Liu, W. Zhang, B. Sun, Y. Chen and H.-J. P. Adler, *Polymer*, 2006, **47**, 1 – 5.

[13] G. Lagaly and S. Ziesmer, *Advances in Colloid and Interface Science*, 2003, **100 − 102**, 105 – 128.

[14] S. Ali and R. Bandyopadhyay, *Langmuir*, 2013, **29**, 12663–12669.

[15] S. Ali and R. Bandyopadhyay, *Applied Clay Science*, 2015, **114**, 85–92.

[16] S. Ali and R. Bandyopadhyay, *Soft Matter*, 2015, DOI: 10.1039/C5SM01700A.

[17] W. Poon, J. Selfe, M. Robertson, S. Ilett, A. Pirie and P. Pusey, *Journal de Physique II*, 1993, **3**, 1075–1086.

[18] S. Manley, J. M. Skotheim, L. Mahadevan and D. A. Weitz, *Physical Review Letters*, 2005, **94**, 218302.

[19] R. Buscall, T. H. Choudhury, M. A. Faers, J. W. Goodwin, P. A. Luckham and S. J. Partridge., *Soft Matter*, 2009, **5**, 1345–1349.

[20] P. Bartlett, L. J. Teece and M. A. Faers, *Physical Review E*, 2012, **85**, 021404.

[21] E. Secchi, S. Buzzaccaro and R. Piazza, *Soft Matter*, 2014, **10**, 5296–5310.

[22] L. Bergstrom, *Journal of Chemical Society, Faraday Transactions*, 1992, **88**, 3201–3211.

[23] A. A. Potanin and W. B. Russel, *Physical Review E*, 1996, **53**, 3702–3709.

[24] H. van Olphen, *John Wiley and Sons Inc.: New York*, 1977, **53**, 230–230.

[25] J. D. F. Ramsay, S. W. Swanton and J. Bunce, *Journal of Chemical Society, Faraday Transactions*, 1990, **86**, 3919–3926.

[26] A. S. Dukhin and P. J. Goetz, *Characterization of Liquids, Nano- and Microparticulates, and Porous Bodies using Ultrasound*, Elsevier: New York, 2010.

[27] P. Snabre and B. Pouligny, *Langmuir*, 2008, **24**, 13338–13347.

[28] É. Guazzelli and J. Hinch, *Annual Review of Fluid Mechanics*, 2011, **43**, 97–116.

[29] R. Secor and C. Radke, *Journal of Colloid and Interface Science*, 1985, **103**, 237 – 244.

[30] E. C. Y. Yan and K. B. Eisenthal, *The Journal of Physical Chemistry B*, 1999, **103**, 6056–6060.

[31] D. Zhou, A. I. Abdel-Fattah and A. A. Keller, *Environmental Science & Technology*, 2012, **46**, 7520–7526.

[32] P. Sollich, F. Lequeux, P. Hébraud and M. E. Cates, *Physical Review Letters*, 1997, **78**, 2020–2023.

[33] M. Delhorme, B. Jonsson and C. Labbez, *Soft Matter*, 2012, **8**, 9691–9704.

[34] E. Zaccarelli, *Journal of Physics: Condensed Matter*, 2007, **19**, 323101.